JOURNAL OF THE AMERICAN CHEMICAL SOCIETY

pubs.acs.org/JACS

Article

Observation of Aromatic $B_{13}(CO)_n^+$ (n = 1−7) as Boron Carbonyl Analogs of Benzene

Rui-Nan Yuan, Jiao-Jiao Chen, Qiang Chen,* Qin-Wei Zhang, Hong Niu, Rui Wei, Zhi-Hong Wei, Xiao-Na Li,* and Si-Dian Li*

Cite This: *J. Am. Chem. Soc.* 2024, 146, 31464−31471

Read Online

ACCESS | Metrics & More | Article Recommendations | Supporting Information

ABSTRACT: CO as a typical σ-donor is one of the most important ligands in chemistry, while planar B_{13}^+ is experimentally known as the most prominent magic-number boron cluster analogous to benzene. Joint gas-phase mass spectroscopy, collision-induced dissociation, and first-principles theory investigations performed herein indicate that B_{13}^+ reacts with CO successively under ambient conditions to form a series of boron carbonyl complexes $B_{13}(CO)_n^+$ up to n = 7, presenting the largest boron carbonyl complexes observed to date with a quasi-planar B_{13}^+ core at the center coordinated by nCO ligands around it. Extensive theoretical analyses unveil both the chemisorption pathways and bonding patterns of these aromatic $B_{13}(CO)_n^+$ monocations which, with three delocalized π bonds well-retained over the slightly wrinkled B_{13}^+ moiety, all prove to be boron carbonyl analogs of benzene tentatively named as boron carbonyl aromatics (BCAs). Their π-isovalent $B_{12}(CO)_n$ (n = 1−6) complexes with a quasi-planar B_{12} coordination center are predicted to be stable neutral BCAs.

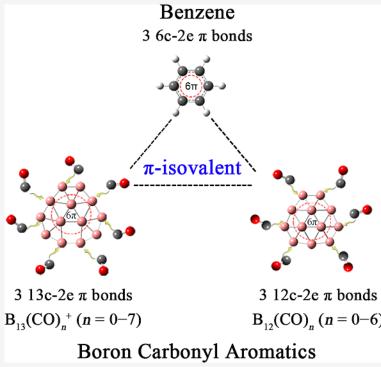

1. INTRODUCTION

Carbon monoxide (CO) with a σ-lone pair on carbon is one of the most important ligands in chemistry and catalysis.[1−3] It is usually used as a σ-donor to coordinate transition metals (TMs) to form various metal carbonyl complexes.[4−7] The σ-lone pair on carbon in a CO ligand (:C≡O) overlaps with the partially occupied d orbitals of the TM center, forming an effective σ-donation coordination bond. Meanwhile, the lowest unoccupied π^*-molecular orbital (LUMO) of CO accepts partial d electrons from the central TM to form π-back-donation interactions.[8−13] Main group metal carbonyl complexes have also been discovered in recent years, including the cubic alkaline-earth metal carbonyl complexes $M(CO)_8$ (M = Ca, Sr, Ba)[14] and $OCBeCO_3$.[15]

Boron ([He]$2s^22p^1$) with partially occupied 2p orbitals exhibits unique structures and bonding due to its prototypical electron deficiency. The first carbonyl borane H_3BCO with a CO ligand was proposed in 1937[16] and the first boron carbonyl molecule BCO was observed in 1991 in which CO acts as a σ-donor to coordinate B.[17] In 1964, Knoth et al. synthesized the first dicarbonyl 1,12-$B_{12}H_{10}(CO)_2$ by reacting $B_{12}H_{12}^{2-}$ with CO under acidic conditions.[18] The crystal structure of this compound, featuring two CO σ-ligands, was measured by X-ray diffraction in 1998.[19] Zhou et al. observed a series of boron carbonyls in solid argon using infrared photodissociation spectroscopy (IRPD) in recent years, including linear BCO,[20] OCBBCO,[21] and BBCO,[22] V-shaped $B(CO)_2$,[23] and rhombus $B_4(CO)_2$.[24] Planar boron carbonyl cation complexes $B(CO)_3^+$, $B(CO)_4^+$, $B_2(CO)_4^+$, and $B_3(CO)_n^+$ (n = 4, 5) were also observed in IRPD experiments,[25−27] and neutral rhombus $B_4(CO)_3$ was characterized in gas phase.[28] Theoretical predictions of larger boron carbonyls including monocyclic aromatic $B_5(CO)_5^-$, $B_6(CO)_6$, and $B_7(CO)_7^+$ have also been reported.[29] These monocyclic $B_n(CO)_n^{-/0/+}$ species were later shown to be obviously less stable than their monocyclic aromatic carbon boronyl counterparts $C_n(BO)_n^{-/0/+/2-}$.[30] However, larger $B_m(CO)_n^{+/0/-}$ boron carbonyl clusters with $m > 4$ or $n > 5$ have not been observed in experiments to date.

It is well-known that the perfect planar C_{2v} B_{13}^+ ($B_3@B_{10}^+$) is a magic-number aromatic boron cluster analogous to benzene.[31] C_{2v} B_{13}^+ exhibits typical fluxional bonding behavior, resulting in a D_{10h} thermally averaged structure,[32] as confirmed by adaptive natural density partitioning (AdNDP) analysis.[33] Alexandrova et al. utilized a circularly polarized infrared laser that could achieve unidirectional rotation of the B_{10} outer ring around the B_3 inner triangle in planar B_{13}^+, forming a photodriven Wankel molecular motor.[34] The reactivity of B_{13}^+ with D_2,[35] HF,[36] N_2O,[37] CO_2,[38] H_2O,[39] and O_2[40] was preliminarily investigated in the late 1980s using an ion cluster beam apparatus, but neither detailed structures of the reactants

Received: June 6, 2024
Revised: October 31, 2024
Accepted: November 1, 2024
Published: November 7, 2024

and products nor the reaction mechanisms were reported during that period. To the best of our knowledge, there have been no experimental or theoretical results on carbonyl complexes of the most prominent aromatic magic-number B_{13}^+ reported to date, leaving an important gap to be explored in the chemistry of boron carbonyl complexes.

Combined gas-phase mass spectrometry, collision-induced dissociation (CID), and first-principles theory investigations performed in this work show that the B_{13}^+ cluster can adsorb CO molecules consecutively under ambient conditions to form a series of boron carbonyl monocations $B_{13}(CO)_n^+$ up to $n = 7$, presenting the largest boron carbonyl complexes observed so far in experiments with a quasi-planar B_{13}^+ moiety at the center coordinated by nCO ligands around it. Extensive theoretical calculations reveal the chemisorption pathways to form these $B_{13}(CO)_n^+$ species which are favorable both thermodynamically and dynamically in gas phase. Detailed AdNDP analyses indicate that these aromatic $B_{13}(CO)_n^+$ (n = 1−7) monocations with three delocalized 13c−2e π-bonds over the B_{13}^+ moiety at the center are the first experimentally identified boron carbonyl analogs of benzene, for which we tentatively propose the name "boron carbonyl aromatics" (BCAs). Their π-isovalent counterparts $B_{12}(CO)_n$ (n = 1−6) with a quasi-planar B_{12} coordination center are predicted to be stable neutral BCAs.

2. METHODS

2.1. Experimental Methods. A homemade reflection time-of-flight mass spectrometer (TOF-MS)[41,42] equipped with a laser ablation ion source, a quadrupole mass filter (QMF),[43] and a linear ion trap (LIT)[44] reactor was used in the experiments. The boron cluster cations (B_n^+) were prepared by laser ablation of a rotating and translating pure boron target made of ^{11}B isotope (99% enriched), in the presence of a 6 atm He carrier gas. A 532 nm pulse laser (second harmonic of Nd^{3+}:yttrium aluminum garnet) with energy of about 3−5 mJ/pulse and a repetition rate of 10 Hz was used. Cluster cations with masses ranging from 50 to 750 amu were generated and detected under these experimental conditions (Figure S1). The cluster cations of $^{11}B_{13}^+$ mass-selected by the QMF entered into the LIT reactor, where they were confined and thermalized by collisions with a pulse of about 4 Pa He gas for 2 ms and then interacted with a pulse of CO reactant gas for a period of time at room temperature. The cluster ions ejected from the LIT reactor were detected by the TOF-MS.

To better comprehend the structural patterns and coordination bonding nature of the experimentally observed $B_{13}(CO)_n^+$ complexes, as a demonstration, detailed CID experiments were performed on the dicarbonyl complex $B_{13}(CO)_2^+$ using a newly developed double-ion-trap apparatus.[45] The $B_{13}(CO)_2^+$ ions were produced by seeding 10% CO in the He cooling gas to react with the cluster-source-generated B_{13}^+ in the first ion trap with a cooling time of about 1.2 ms. The generated $B_{13}(CO)_2^+$ ions were then mass-selected to interact with Xe in the second ion trap (run at the collision cell mode). The pressure of Xe was low (∼70 mPa) and the time period of collisions was short (∼20 μs). The estimated average collision[46] number of 0.08 between $B_{13}(CO)_2^+$ and Xe indicates that multiple collisions should be negligible in the CID experiments. The center-of-mass collisional energy (E_{cm}) between $B_{13}(CO)_2^+$ and Xe was computed by using $E_{cm} = E_k \times m/(m + M)$, in which E_k is the kinetic energy of $B_{13}(CO)_2^+$ and M and m are the masses of $B_{13}(CO)_2^+$ and Xe, respectively.

2.2. Theoretical Methods. Extensive density functional theory calculations at PBE0/6-311+G(d,p) level[47,48] were carried out using the Gaussian 16 program[49] to optimize the structures of reactant B_{13}^+ and products $B_{13}(CO)_n^+$ (n = 1−7) as well as the corresponding intermediates (IMs) and transition states (TSs). The PBE0 functional has been used widely to characterize B_n^- monoanions observed in photoelectron spectroscopy experiments[50−52] and to simulate the IRPD of B_{13}^+.[53] More accurate single-point energy calculations were performed at the coupled cluster CCSD(T)/6-311+G(d,p) level[54−57] at PBE0 geometries, with the small calculated T_1 diagnostic values between 0.019 and 0.024. Vibrational frequency checks were performed to ensure that all the IMs and TSs obtained are true minima and transition states of the systems, respectively. Intrinsic reaction coordinate calculations were carried out to make sure that each TS leads to two appropriate IMs.[58,59] Born−Oppenheimer molecular dynamics (BOMD) simulations were performed on $B_{13}(CO)_n^+$ (n = 1−7) for 100 ps using the CP2K software package suite[60] with the GTH-PBE0 pseudopotentials and TZVP-MOLOPT-PBE-GTH basis sets.[61,62] Detailed bonding analyses were carried out employing the widely used AdNDP approach.[63] Energy decomposition analyses with natural orbitals for chemical valence (EDA-NOCV)[64−66] were performed on $B_{13}CO^+$ (**1A**) at the PBE0/TZ2P level with the ADF 2022 program package[67] using the zeroth-order regular approximation.[68−70]

3. RESULTS AND DISCUSSION

3.1. Cluster Reactivity Measurements. The measured TOF mass spectra for the reactions of B_{13}^+ clusters with up to seven CO molecules are collectively presented in Figure 1. Upon the interaction of B_{13}^+ with 184 mPa CO for 2 ms, two product signals of $B_{13}CO^+$ and $B_{13}(CO)_2^+$ were clearly observed (Figure 1b). With the increase of CO pressure to 378 mPa, the intensities of products $B_{13}CO^+$ and $B_{13}(CO)_2^+$

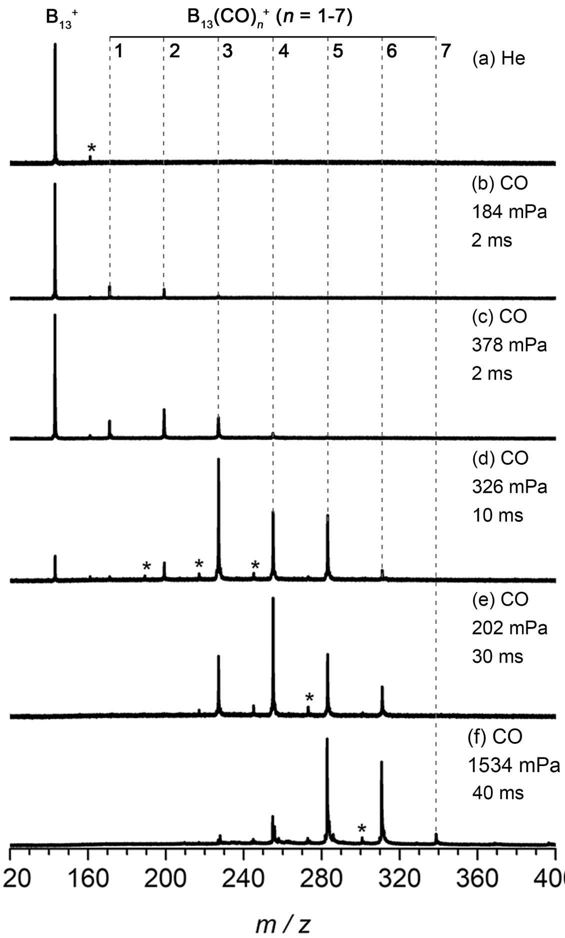

Figure 1. Measured TOF mass spectra for the reactions of mass-selected B_{13}^+ with (a) He and (b−f) CO molecules. The CO reactant gas pressures and reaction times are indicated in mPa and ms, respectively. The weak mass signals marked with asterisks are due to existence of water impurities in the reaction system.

https://doi.org/10.1021/jacs.4c07680
J. Am. Chem. Soc. 2024, 146, 31464−31471

increased significantly. The emergence of the third and fourth product signals at $B_{13}(CO)_3^+$ and $B_{13}(CO)_4^+$ indicates that $B_{13}(CO)_2^+$ can further react with one or two more CO molecules successively (Figure 1c).

Given the fact that the signal intensity of B_{13}^+ remained strong at the reaction time of 2 ms (Figure 1b,c), longer reaction times and higher reactant gas pressures were used to explore the possibility of B_{13}^+ to interact with more CO molecules. When the reaction time was elongated to 10 ms, the signal intensities of B_{13}^+, $B_{13}(CO)^+$, and $B_{13}(CO)_2^+$ decreased remarkably, the signals of $B_{13}(CO)_3^+$ and $B_{13}(CO)_4^+$ increased obviously, while two new product peaks corresponding to $B_{13}(CO)_5^+$ and $B_{13}(CO)_6^+$ could be clearly identified (Figure 1d). By adjusting the reaction time to 30 ms, we observed a depletion of the $B_{13}(CO)_n^+$ (n = 0−2) signals, a notable decrease in $B_{13}(CO)_3^+$ and an enhancement of $B_{13}(CO)_4^+$ as the predominant peak in the resulting mass spectrum (Figure 1e). When the reaction time was further extended to 40 ms and CO pressure increased to 1534 mPa, a weak product signal corresponding to $B_{13}(CO)_7^+$ was distinctly identified, but no mass signal beyond was detected for $B_{13}(CO)_8^+$ (Figure 1f). The experimental results observed above show that B_{13}^+ can adsorb up to seven CO molecules consecutively in the following chemisorption reaction

$$B_{13}^+ + n\mathrm{CO} \rightarrow B_{13}(\mathrm{CO})_n^+ \ (n = 1-7) \qquad (1)$$

The measured CID mass spectra depicted in Figure S2 clearly indicate that, with the center-of-mass collisional energies of E_{cm} = 2.0 and 3.6 eV, the $B_{13}(CO)_2^+$ adduct loses the first CO molecule to generate $B_{13}(CO)^+$ (Figure S2b) and the second CO molecule to produce B_{13}^+ (Figure S2c), respectively in the following CID process

$$B_{13}(\mathrm{CO})_2^+ \xrightarrow{\mathrm{CID}} B_{13}(\mathrm{CO})_{(2-n)}^+ + n\mathrm{CO} \ (n = 1, 2) \qquad (2)$$

The CID results provide strong experimental evidence that the two CO ligands in $B_{13}(CO)_2^+$ are indeed adsorbed molecularly to the B_{13}^+ coordination center, rather than being chemically activated or incorporated into the skeleton of B_{13}^+ moiety, similar to the situations in various well-known metal carbonyl complexes.[4−7]

Based on a least-squares fitting procedure (Figure 2), the pseudo-first-order rate constants (k_1) for the reactions of $B_{13}(CO)_n^+$ (n = 0−3) with CO were estimated to be $k_1 = 4.26 \times 10^{-12}$, 33.64×10^{-12}, 11.1×10^{-12}, and 2.98×10^{-12} cm^3 molecule^{-1} s^{-1} for n = 0, 1, 2, and 3, corresponding to the reaction efficiencies of Φ = 0.62%, 4.99%, 1.66%, and 0.45%, respectively. The combined reaction rate constant of $B_{13}(CO)_5^+$ and $B_{13}(CO)_6^+$ was estimated to be $k_1 = 6.20 \times 10^{-12}$ (Φ = 0.96%) in Figure 2 due to their weak mass intensities. Reaction (1) possesses rate constants comparable to the N_2-adsorption processes $Rh_3D_n^- + N_2 = Rh_3D_nN_2^-$ (n = 1, 2, 3)[71] which appear to be slightly smaller than the rate constants of CO adsorption on Au_{15}^+ monocation.[72,73]

As comparisons, the gas-phase reactions of B_{13}^+ with H_2, N_2, CO_2, CH_4, C_2H_6, and O_2 were also conducted in this work. Their measured TOF mass spectra collectively shown in Figure S3 clearly indicate that B_{13}^+ is unreactive with these small molecules, demonstrating the unique coordination capacity of CO as a σ-donor to B_{13}^+.

3.2. Chemisorption Pathway Analyses. The optimized structures of boron carbonyl products $B_{13}(CO)_n^+$ (n = 1−8) (Figures S4−S7) and relevant chemisorption pathways of B_{13}^+

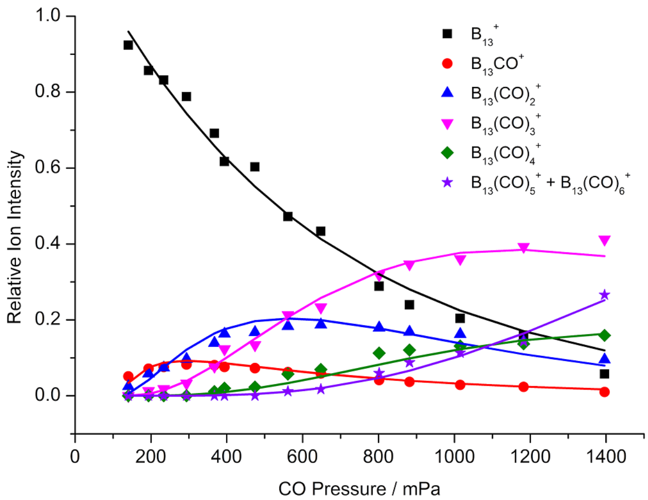

Figure 2. Variation of the measured relative signal intensities of reactant and product ions with respect to effective reactant gas pressures in the reactions of $B_{13}^+ + n$CO = $B_{13}(CO)_n^+$ (n = 0−6). The solid lines are fitted to experimental data points with the approximation of pseudo-first-order reaction mechanisms. Combined signal intensities of $B_{13}(CO)_5^+$ and $B_{13}(CO)_6^+$ are plotted in purple stars.

with nCO molecules (Figures S8−S30) were obtained at PBE0 level, with the relative energies refined at CCSD(T). The low-lying isomers of $B_{13}(CO)_n^+$ (n = 1−8) complexes are denoted as n**A**, n**B**, and n**C** etc. based on their relative energy orders. It is clear that CO ligands prefer to be chemically adsorbed on the outer B_{10} ring of the B_{13}^+ ($B_3@B_{10}^+$) moiety in a terminal coordination manner, forming effective B−CO σ-donation and weak π-backdonation interactions between the B_{13} core and its CO ligands, without destroying the structural integrity of the B_{13}^+ core.

As shown in Figures 3 and S8a, the first CO coordinates B_{13}^+ at a tricoordinate B apex in the outer B_{10} ring without an energy barrier, forming the most stable adduct complex C_1 $B_{13}(CO)^+$ (**1A**) with the chemisorption energy of 1.17 eV at PBE0. The almost degenerate complex **1C** which lies only 0.06 eV less stable than **1A** at CCSD(T) can be barrierlessly generated in gas phase and spontaneously converted into **1A** (Figure S8b), but the generation of the second lowest-lying **1B** from B_{13}^+ encounters a positive energy barrier to overcome. In the stable complex **1A**, the migration of the CO ligand (Figure S8c), extrusion of one B atom from the skeleton of B_{13} (Figure S8b), and breakage of the C≡O triple bond (Figure S9) all encounter positive barriers. Thus, the observed product $B_{13}(CO)^+$ is indeed the CO complex (**1A**) as evidenced in the CID mass spectroscopy shown in Figure S2, rather than the global minimum or any other low-lying isomers of the system.

The second CO molecule coordinates to a tricoordinate B site of **1A** in a barrier-free pathway to produce C_2 $B_{13}(CO)_2^+$ (**2A**) or C_1 $B_{13}(CO)_2^+$ (**2B**) (Figures 3a and S10a) with the chemisorption energies of 1.23 eV for **2A** and 1.17 eV for **2B** at CCSD(T), respectively. The conversion of **2B** to the more stable species **2A** via CO migration must overcome a substantial energy barrier of 1.80 eV at CCSD(T) (Figure S10b) that is high enough to impede the transformation between **2A** and **2B**. We notice that both the extrusion of one boron atom from **2A** (Figures S10c) and activation of a C≡O bond in **2A** (Figure S11) encounter large energy barriers, well

https://doi.org/10.1021/jacs.4c07680
J. Am. Chem. Soc. 2024, 146, 31464−31471

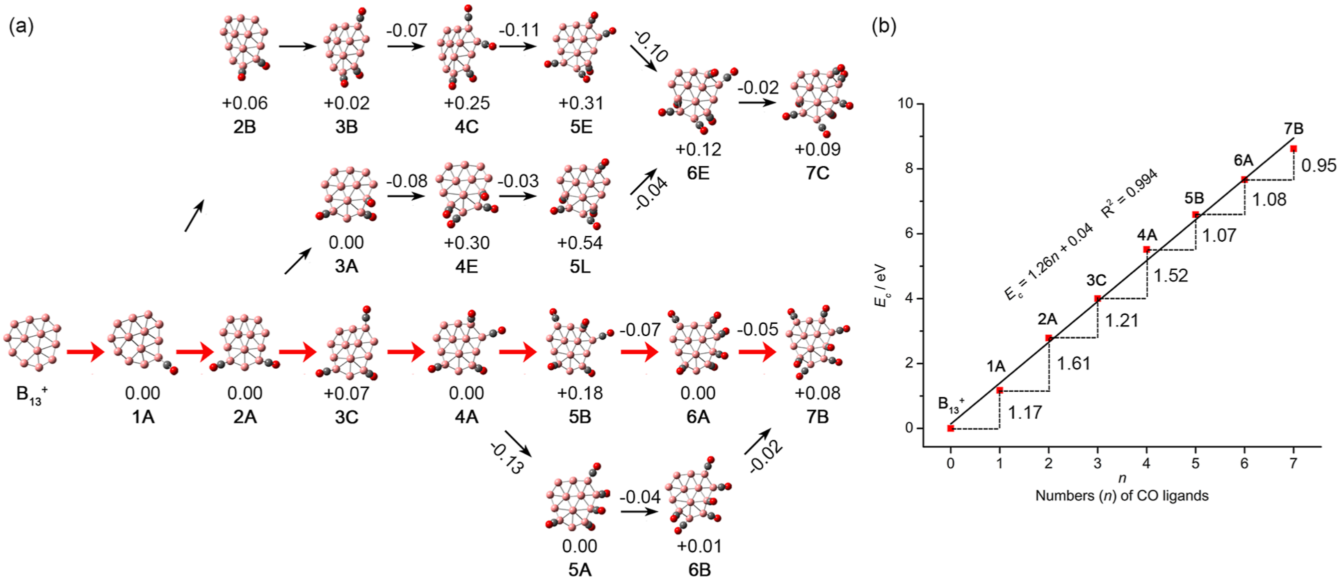

Figure 3. (a) Chemisorption pathways of the $B_{13}(CO)_n^+$ complex series (n = 1−7) obtained at PBE0/6-311+G(d,p) level, with the relative energies and energy barriers indicated in eV at CCSD(T)//PBE0. The red arrows represent the most favorable chemisorption pathway. The calculated energy barriers of TSs with respect to the separate reactants [CO and $B_{13}(CO)_{n-1}^+$ (n = 1−7)] are labeled above the arrows. (b) Calculated chemisorption energies $E_c = (E_{B_{13}^+} + nE_{CO}) - E_{B_{13}(CO)_n^+}$ of **1A**, **2A**, **3C**, **4A**, **5B**, **6A**, and **7B** complexes with respect to reaction (**1**) in the most favorable chemisorption pathway at PBE0.

supporting the CID experimental observation that the two CO ligands are adsorbed molecularly to the B_{13}^+ coordination center in $B_{13}(CO)_2^+$ (Figure S2).

When the third CO molecule approaches **2A**, it can be tightly anchored to the B_{13}^+ core via either a tetracoordinated B or a tricoordinated B of **2A**, resulting in the barrier-free formation of $B_{13}(CO)_3^+$ (**3A**) and $B_{13}(CO)_3^+$ (**3C**) (Figures 3 and S12) with the chemisorption energies of 0.87 and 0.80 eV at CCSD(T), respectively. Similarly, **2B** can also barrierlessly capture the third CO through its tricoordinate B, preferentially forming **3B** (Figure S13) with a binding energy of 0.91 eV at CCSD(T). **3B** and **3C** are slightly higher in energy than the most stable **3A** by 0.02 and 0.07 eV, respectively. Hindered by large CO migration energy barriers greater than 1.34 eV at CCSD(T) (Figure S14), the close-lying **3A**, **3B**, and **3C** may coexist in the experimentally observed mass signal of $B_{13}(CO)_3^+$ (Figure 1).

The coordination of the fourth CO onto a tricoordinate B of **3C** barrierlessly generates the most stable complex $B_{13}(CO)_4^+$ complex (**4A**) (Figures 3 and S15) with a binding energy of 0.99 eV at CCSD(T). The fifth CO can coordinate **4A** readily to produce the stable complex of $B_{13}(CO)_5^+$ (**5B**) (Figures 3 and S16) with a binding energy of 0.64 eV. The resulting **5B** captures the sixth CO via its tetracoordinate B site, forming an IM complex (**I24**) (Figure S17) with a binding energy of 0.14 eV. Consequently, the negative energy barrier of −0.07 eV can be easily overcome to yield the most stable complex $B_{13}(CO)_6^+$ (**6A**) with the adsorption energy of 0.74 eV at CCSD(T). As the seventh CO approaches **6A**, an IM complex (**I27**) with a binding energy of 0.13 eV is generated via coordination of a CO to a tricoordinate B site of 6A (Figure S18), yielding the dynamically favorable $B_{13}(CO)_7^+$ (**7B**) rather than (**7A**) because a positive barrier of 0.06 eV is encountered to generate the latter (Figure S18). Product **7B** can also be formed along the reaction pathway **4A** → **5A** → **6B** → **7B** (Figures S16, S19, and S20); however, it is less favorable because the energies of the involved TSs are less negative than those in the pathway **4A** → **5B** → **6A** → **7B**. It is worth noticing that **5B** is 0.18 eV higher in energy than the most stable complex **5A**. Similarly, for complex $B_{13}(CO)_7^+$, **7B** is marginally higher by 0.08 eV with respect to **7A**. Related conversion from **5B** to **5A** or from **7B** to **7A** is challenging due to the substantial CO migration barriers. It is also noticed that **7B** has the smallest adsorption energy of 0.95 eV at PBE0 among the $B_{13}(CO)_n^+$ series (n = 1−7) (Figure 3b), well supporting the fact that $B_{13}(CO)_7^+$ has the lowest mass signal intensity observed in Figure 1f.

Starting from **3A** or **3B**, the final boron carbonyl complex $B_{13}(CO)_7^+$ (**7C**) can also be produced exothermically (**3A** → **4E** → **5L** → **6E** → **7C** and **3B** → **4C** → **5E** → **6E** → **7C**; Figures S21−S27). The species **4E**/**4C**, **5L**/**5E**, **6E**, and **7C**, although less stable than their counterparts originated from **3C**, are expected to coexist in the experiments as minor isomers. This is supported by the fact that the mass signals of $B_{13}(CO)_3^+$ and $B_{13}(CO)_4^+$ disappeared almost completely in experiments (Figure 1f) and there are obvious energy barriers for CO migrations in these species (Figures S14 and S28).

When the eighth CO molecule approaches **7B** or **7C**, the formation of stable complexes $B_{13}(CO)_8^+$ (**8A** and **8C**) encounters obvious positive energy barriers (+0.10 eV for **7B** + CO → **I51**→ **TS61** → **8A** and +0.45 eV for **7C** + CO → **I52** → **TS62** → **8C** at CCSD(T); Figures S29 and S30. With entropy effect considered at 298 K, the corresponding energy barriers are increased to +0.45 eV and +0.81 eV, respectively). The Rice−Ramsperger−Kassel−Marcus (RRKM) theory and RRKM-based variational transition-state theory[74] were used to estimate the rate constants of internal conversion (k_{int}) and the desorption of CO (k_d) from the IM complexes **I51** and **I52**, respectively. The rates of CO desorption from **I51** to **7B** (k_d = 4.4 × 10^{11} s^{-1}) and from **I52** to **7C** (k_d = 1.2 × 10^{11} s^{-1}) are much faster than the rates of internal conversions from **I51** to **TS61** (k_{int} = 6.3 × 10^9 s^{-1}) and from **I52** to **TS62** (k_{int} = 1.5 × 10^5 s^{-1}), respectively. Therefore, the eighth CO in **I51** and **I52** can be easily evaporated into gas phase rather than overcome

https://doi.org/10.1021/jacs.4c07680
J. Am. Chem. Soc. 2024, 146, 31464−31471

the positive barriers to form **8A** and **8C**. These results are well in agreement with the experimental observation that no mass signal of $B_{13}(CO)_8^+$ was detected in experiments (Figure 1f). Overall, our calculations effectively interpret the experimental findings that B_{13}^+ can consecutively adsorb up to seven CO molecules.

With an overall energy release of 8.61 eV in the whole chemisorption process, the pathway $\mathbf{B_{13}^+} \rightarrow$ **1A** $\rightarrow$ **2A** $\rightarrow$ **3C** $\rightarrow$ **4A** $\rightarrow$ **5B** $\rightarrow$ **6A** $\rightarrow$ **7B** is predicted to be the most favorable one both thermodynamically and dynamically. The CID experimental results shown in Figure S2 indicate that the coordinations of CO to B_{13}^+ are irreversible processes unless external energies such as molecular collisions or irradiation are provided to desorb the CO ligands from the complexes. As shown in Figure 3b, the chemisorption energies $E_c = (E_{B_{13}^+} + nE_{CO}) - E_{B_{13}(CO)_n^+}$ of $B_{13}(CO)_n^+$ monocations with respect to reaction (**1**) increase almost perfectly linearly with the numbers (n) of CO ligands involved in the complexes, with an approximate average chemisorption energy per CO of E_c/CO = 1.26 eV at PBE0, suggesting that the seven coordination sites on the outer B_{10} ring absorb CO molecules almost independently.

3.3. Molecular Dynamics Simulations. Extensive BOMD simulations were performed to check the dynamic stability of the concerned species in the most favorable chemisorption pathway highlighted with red arrows in Figure 3a. Interestingly, these species all appear to be dynamically stable at 500 K in 100 ps with small calculated root-mean-square-deviations and maximum bond length deviations obtained, except **1A** which coexists with **1C** spontaneously at 300 K (Figure S31).

3.4. Bonding Pattern Analyses. To better comprehend the high stability of these boron carbonyl complexes, detailed AdNDP analyses were performed to unveil their bonding patterns. As a comparison shown in Figure S32, the experimentally characterized perfectly planar C_{2v} B_{13}^+ bare cluster possesses 10 2c−2e σ bonds along the B_{10} outer ring, 1 3c−2e σ bond on the B_3 triangle at the center, 5 3c−2e σ bonds between the outer ring and inner ring, and 3 completely delocalized 13c−2e π-bonds over the molecular plane, making it π-aromatic in nature analogous to benzene. Interestingly, as clearly shown in Figure S33a, similar to B_{13}^+, the slightly wrinkled C_1 $B_{13}(CO)^+$ (**1A**) also contains 10 2c−2e σ-bonds along the outer B_{10} ring, 1 3c−2e σ-bond on the central B_3 triangle, 5 partially delocalized σ-bonds between the outer and inner rings over on the B_{13}^+ core, and most importantly, 3 totally delocalized 13c−2e π-bonds over the B_{13} moiety (Figure 4), making $B_{13}(CO)^+$ (**1A**) also π-aromatic in nature analogous to benzene. Coordination of one CO ligand with a σ-lone-pair on the C end introduces one 2c−2e σ-donation bond between B_{13}^+ and CO into the system, but without changing the fundamental bonding patterns of the B_{13}^+ moiety. As collectively demonstrated in Figures 4b−h and S33−S36, with the introduction of nCO ligands with n σ-lone pairs into the systems, despite slight structural distortions to the B_{13}^+ moiety and the formation of n 2c−2e C−B σ-donation bonds between B_{13}^+ and its nCO ligands, the 3 13c−2e π-bonds over the slightly wrinkled B_{13}^+ core have been well-retained throughout the $B_{13}(CO)_n^+$ series (n = 1−7), rendering π-aromaticity and extra stability to the systems and making them boron carbonyl analogs to benzene. It is also noticed that the strong C≡O triple bonding interactions (1 2c−2e C−O σ + 2 2c−2e C−O π) in the CO ligands are well maintained throughout the $B_{13}(CO)_n^+$ series (n = 1−7).

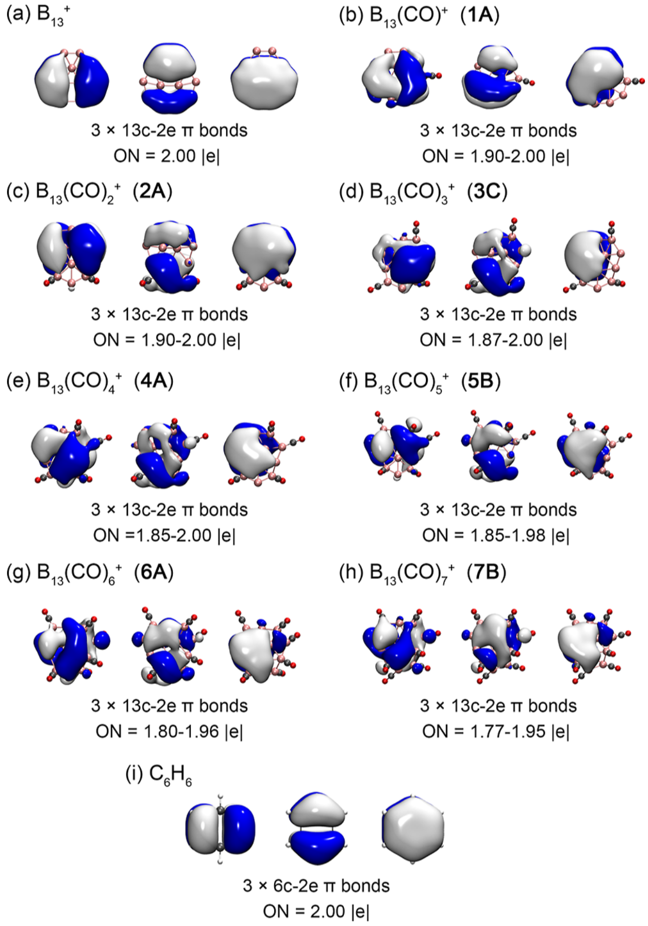

Figure 4. AdNDP π-bonding patterns of (a) B_{13}^+ and (b−h) $B_{13}(CO)_n^+$ (n = 1−7), in comparison with that of benzene (i) C_6H_6, with the occupation numbers indicated.

3.5. Strong σ-Donations and Weak π-Back-Donations. As demonstrated in Figure S37 and Table S1, detailed EDA-NOCV analyses on $B_{13}(CO)^+$ (**1A**) using B_{13}^+ and CO as interacting fragments indicate that one effective σ-donation (HOMO − 15) which contributes 64.9% to the overall orbital interactions (ΔE_{orb}) and two weak π-back-donations (HOMO and HOMO − 7) which contribute 15.0% and 9.2%, respectively, coexist in the coordination interactions between B_{13}^+ and CO, with the strong σ-donation coordination interactions well reflected in the 2c−2e B−C σ-bond in AdNDP analysis presented in Figure S33a. It is noticed that both of the two weak π-back-donations HOMO and HOMO − 7 in which the two degenerate unoccupied π*-LUMOs of the CO ligand accept partial electrons from the B_{13}^+ core mainly contain contributions from the HOMO (75.4%) and HOMO − 6 (79.4%) of the B_{13}^+ core which mainly react with the CO ligand via the partially occupied 2p atomic orbitals of the tricoordinate B atom (p $\rightarrow$ π-back-donations), similar to but different from the situations in the first borylene dicarbonyl complex synthesized by Braunschweig et al.[75] where a boron atom binds CO with strong π-back-donation from the boron to CO.

3.6. Prediction of Neutral BCAs $B_{12}(CO)_n$ (n = 1−6). Using the previously experimentally observed π-aromatic C_{3v} B_{12} (B_3@B_9) as coordination center which is the well-known boron analog of benzene,[76] we predict a series of stable neutral BCAs $B_{12}(CO)_n$ (n = 1−6) at PBE0, as shown in Figure 5. As

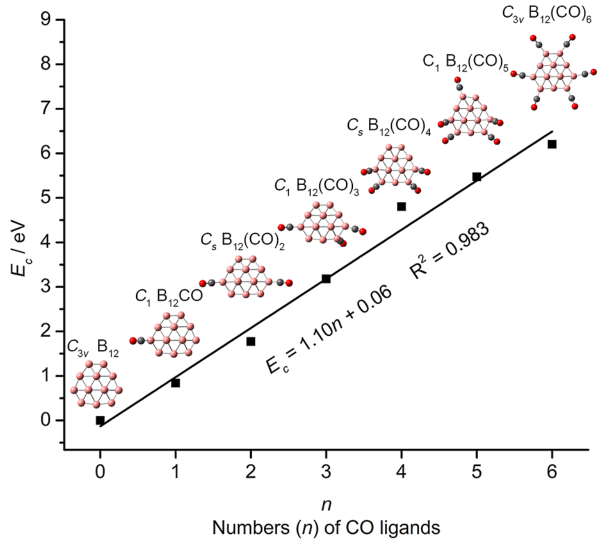

Figure 5. Optimized structures and calculated chemisorption energies $E_c = (E_{B12} + nE_{CO}) - E_{B12(CO)n}$ of neutral C_1 $B_{12}(CO)$ (^1A), C_s $B_{12}(CO)_2$ ($^1A'$), C_1 $B_{12}(CO)_3$ (^1A), C_s $B_{12}(CO)_4$ ($^1A'$), C_1 $B_{12}(CO)_5$ (^1A), and C_{3v} $B_{12}(CO)_6$ ($^1A_1$) complexes with respect to reaction (**2**) at PBE0 level.

π-isovalent species of the $B_{13}(CO)_n^+$ monocations observed above, the optimized neutral quasi-planar C_1 $B_{12}(CO)$, C_s $B_{12}(CO)_2$, C_1 $B_{12}(CO)_3$, C_s $B_{12}(CO)_4$, C_1 $B_{12}(CO)_5$, and C_{3v} $B_{12}(CO)_6$ can be systematically generated with one to six CO molecules coordinating the B_{12} center in the outer B_9 ring. Encouragingly, as shown in Figure 5, the chemisorption energies $E_c = (E_{B12} + nE_{CO}) - E_{B12(CO)n}$ of neutral $B_{12}(CO)_n$ with respect to reaction (**3**)

$$B_{12} + nCO \rightarrow B_{12}(CO)_n \ (n = 1-6) \quad (3)$$

also exhibit a nice linear relationship with the number of CO ligands in the complexes, with the average chemisorption energy per CO of E_c/CO = 1.10 eV at PBE0 which is slightly lower than that of the $B_{13}(CO)_n^+$ monocations. More interestingly, detailed AdNDP analyses clearly indicate that these slightly wrinkled neutral $B_{12}(CO)_n$ (n = 1−6) complexes well inherit the three delocalized 12c−2e π bonds of the parent bare cluster C_{3v} B_{12} (Figure S38), rendering π-aromaticity to these systems which could be potentially synthesized and characterized in future experiments. The B_3 triangle at the center of both $B_{13}(CO)_n^+$ and $B_{12}(CO)_n$ series helps render σ + π dual-aromaticity to the systems, making these concentric bicyclic BCAs stable both thermodynamically and dynamically.

4. CONCLUSIONS

In summary, joint experimental and theoretical investigations performed in this work indicate that B_{13}^+ can react with CO molecules consecutively at ambient conditions to generate a series of aromatic boron carbonyls $B_{13}(CO)_n^+$ (n = 1−7) analogous to benzene. Similar to the situation in TM carbonyls, both effective σ-donations and weak π-back-donations coexist between B_{13}^+ and its CO ligands, indicating that B atoms exhibit transition-metal-like behavior in these BCAs. Stable neutral BCAs $B_{12}(CO)_n$ (n = 1−6) have also been predicted in this work. Macroscopic syntheses and isolations of such stable BCAs would help facilitate their applications in chemistry and catalysis and further enrich the chemistry of boron.

■ ASSOCIATED CONTENT

Supporting Information

The Supporting Information is available free of charge at https://pubs.acs.org/doi/10.1021/jacs.4c07680.

Details of experimental and computational and results (spectra and calculated structures and reaction mechanisms) (PDF)

■ AUTHOR INFORMATION

Corresponding Authors

Qiang Chen − *Institute of Molecular Science, Shanxi University, Taiyuan 030006, P. R. China*; Email: chenqiang@sxu.edu.cn

Xiao-Na Li − *Key Laboratory of Cluster Science of Ministry of Education, School of Chemistry and Chemical Engineering, Beijing Institute of Technology, Beijing 102488, P. R. China*; orcid.org/0000-0002-0316-5762; Email: xiaonali@bit.edu.cn

Si-Dian Li − *Institute of Molecular Science, Shanxi University, Taiyuan 030006, P. R. China*; orcid.org/0000-0001-5666-0591; Email: lisidian@sxu.edu.cn

Authors

Rui-Nan Yuan − *Institute of Molecular Science, Shanxi University, Taiyuan 030006, P. R. China*

Jiao-Jiao Chen − *School of Mathematics and Physics, North China Electric Power University, Beijing 102206, P. R. China*; orcid.org/0009-0008-7869-8660

Qin-Wei Zhang − *Institute of Molecular Science, Shanxi University, Taiyuan 030006, P. R. China*

Hong Niu − *Institute of Molecular Science, Shanxi University, Taiyuan 030006, P. R. China*

Rui Wei − *Institute of Molecular Science, Shanxi University, Taiyuan 030006, P. R. China*

Zhi-Hong Wei − *Institute of Molecular Science, Shanxi University, Taiyuan 030006, P. R. China*; orcid.org/0000-0002-9460-7908

Complete contact information is available at: https://pubs.acs.org/10.1021/jacs.4c07680

Notes

The authors declare no competing financial interest.

■ ACKNOWLEDGMENTS

This work was supported by the National Natural Science Foundation of China (Grant Nos. 22003034, 22373061, 22022308, and 92161116). The authors sincerely thank the Institute of Chemistry, Chinese Academy of Sciences for the use of the CID apparatus in this work.

■ REFERENCES

(1) Tian, Q. Q.; Yin, X.; Sun, R. J.; Wu, X. F.; Li, Y. H. The lower the better: Efficient carbonylative reactions under atmospheric pressure of carbon monoxide. *Coord. Chem. Rev.* **2023**, *475*, 214900.
(2) Zhang, S. K.; Neumann, H.; Beller, M. Synthesis of α,β-unsaturated carbonyl compounds by carbonylation reactions. *Chem. Soc. Rev.* **2020**, *49*, 3187−3210.
(3) Peng, J. B.; Geng, H. Q.; Wu, X. F. The chemistry of CO: carbonylation. *Chem* **2019**, *5*, 526−552.

(4) Macchi, P.; Sironi, A. Chemical bonding in transition metal carbonyl clusters: complementary analysis of theoretical and experimental electron densities. *Coord. Chem. Rev.* **2003**, *238*, 383−412.
(5) Armentrout, P. B. 18 electrons and counting. *Science* **2018**, *361*, 849−850.
(6) Lupinetti, A. J.; Fau, S.; Frenking, G.; Strauss, S. H. Theoretical analysis of the bonding between CO and positively charged atoms. *J. Phys. Chem. A* **1997**, *101*, 9551−9559.
(7) Diefenbach, A.; Bickelhaupt, F. M.; Frenking, G. The nature of the transition metal-carbonyl bond and the question about the valence orbitals of transition metals. A bond-energy decomposition analysis of $TM(CO)_6^q$ ($TM^q = Hf^{2-}$, Ta^-, W, Re^+, Os^{2+}, Ir^{3+}). *J. Am. Chem. Soc.* **2000**, *122*, 6449−6458.
(8) Frenking, G.; Fröhlich, N. The nature of the bonding in transition-metal compounds. *Chem. Rev.* **2000**, *100*, 717−774.
(9) Jiang, L.; Xu, Q. Experimental and theoretical evidence for the formation of zinc tricarbonyl in solid argon. *J. Am. Chem. Soc.* **2005**, *127*, 8906−8907.
(10) Jin, J.; Yang, T.; Xin, K.; Wang, G.; Jin, X.; Zhou, M.; Frenking, G. Octacarbonyl anion complexes of group three transition metals $[TM(CO)_8]^-$ (TM = Sc, Y, La) and the 18-Electron Rule. *Angew. Chem., Int. Ed.* **2018**, *57*, 6236−6241.
(11) Fortes, A. D.; Parker, S. F. Structure and spectroscopy of iron pentacarbonyl, $Fe(CO)_5$. *J. Am. Chem. Soc.* **2022**, *144*, 17376−17386.
(12) Frenking, G.; Fernández, I.; Holzmann, N.; Pan, S.; Krossing, I.; Zhou, M. Metal-CO bonding in mononuclear transition metal carbonyl complexes. *JACS Au* **2021**, *1*, 623−645.
(13) Chi, C.; Wang, J. Q.; Hu, H. S.; Zhang, Y. Y.; Li, W. L.; Meng, L.; Luo, M.; Zhou, M.; Li, J. Quadruple bonding between iron and boron in the $BFe(CO)_3^-$ complex. *Nat. Commun.* **2019**, *10*, 4713.
(14) Wu, X.; Zhao, L.; Jin, J.; Pan, S.; Li, W.; Jin, X.; Wang, G.; Zhou, M.; Frenking, G. Observation of alkaline earth complexes $M(CO)_8$ (M = Ca, Sr, or Ba) that mimic transition metals. *Science* **2018**, *361*, 912−916.
(15) Chen, M.; Zhang, Q.; Zhou, M.; Andrada, D. M.; Frenking, G. Carbon monoxide bonding with BeO and $BeCO_3$: surprisingly high CO stretching frequency of $OCBeCO_3$. *Angew. Chem., Int. Ed.* **2015**, *54*, 124−128.
(16) Burg, A. B.; Schlesinger, H. I. Hydrides of boron VII Evidence of the transitory existence of borine (BH_3) borine carbonyl and borme trimethylammine. *J. Am. Chem. Soc.* **1937**, *59*, 780−787.
(17) Hamrick, Y. M.; Vanzee, R. J.; Godbout, J. T.; Weltner, W.; Lauderdale, W. J.; Stanton, J. F.; Bartlett, R. J. The boron-carbon monoxide molecule. *J. Phys. Chem.* **1991**, *95*, 2840−2844.
(18) Knoth, W. H.; Sauer, J. C.; Miller, H. C.; Muetterties, E. L. Diazonium and carbonyl derivatives of polyhedral boranes. *J. Am. Chem. Soc.* **1964**, *86*, 115−116.
(19) Fox, M. A.; Howard, J. A. K.; Moloney, J. M.; Wade, K. Molecular structures of 1,12-$B_{12}H_{10}(CO)_2$ and its dihydrate 1,12-$B_{12}H_{10}[C(OH)_2]$-a novel bis-carbene complex. *Chem. Commun.* **1998**, 2487−2488.
(20) Zhou, M.; Tsumori, N.; Andrews, L.; Xu, Q. A. Infrared spectra of BCO, $B(CO)_2$, and OCBBCO in solid argon. *J. Phys. Chem. A* **2003**, *107*, 2458−2463.
(21) Zhou, M.; Tsumori, N.; Li, Z.; Fan, K.; Andrews, L.; Xu, Q. OCBBCO: A neutral molecule with some boron−boron triple bond character. *J. Am. Chem. Soc.* **2002**, *124*, 12936−12937.
(22) Zhou, M.; Wang, Z. X.; Schleyer, P. v. R.; Xu, Q. Experimental and theoretical characterization of a triplet boron carbonyl compound: BBCO. *ChemPhysChem* **2003**, *4*, 763−766.
(23) Burkholder, T. R.; Andrews, L. Reaction of boron atoms with CO. Matrix infrared spectra of BCO, $(BCO)_2$, and $B(CO)_2$. *J. Phys. Chem.* **1992**, *96*, 10195−10201.
(24) Zhou, M.; Xu, Q.; Wang, Z. X.; Schleyer, P. v. R. $B_4(CO)_2$: A new, observable σ-π diradical. *J. Am. Chem. Soc.* **2002**, *124*, 14854−14855.
(25) Jin, J. Y.; Wang, G. J.; Zhou, M. F. Infrared Photodisssociation Spectroscopy of Boron Carbonyl Cation Complexes. *Chin. J. Chem. Phys.* **2016**, *29*, 47−52.
(26) Jin, J.; Wang, G.; Zhou, M. Boron carbonyl analogues of hydrocarbons: An infrared photodissociation spectroscopic study of $B_3(CO)_n^+$ (n = 4−6). *J. Phys. Chem. A* **2018**, *122*, 2688−2694.
(27) Jin, J.; Wang, G.; Zhou, M.; Andrada, D. M.; Hermann, M.; Frenking, G. The $[B_3(NN)_3]^+$ and $[B_3(CO)_3]^+$ complexes featuring the smallest π-aromatic species B_3^+. *Angew. Chem., Int. Ed.* **2016**, *55*, 2078−2082.
(28) Zhao, Y.; Wang, T.; Wang, C.; Zhang, Z.; Zheng, H.; Jiang, S.; Yan, W.; Xie, H.; Li, G.; Yang, J.; Wu, G.; Zhang, W.; Dai, D.; Zheng, X.; Fan, H.; Jiang, L.; Yang, X.; Zhou, M. Ligand-induced tuning of the electronic structure of rhombus tetraboron cluster. *ChemPhysChem* **2022**, *23*, No. e202200060.
(29) Wu, H. S.; Jiao, H. J.; Wang, Z. X.; Schleyer, P. v. R. Monocyclic boron carbonyls: Novel aromatic compounds. *J. Am. Chem. Soc.* **2003**, *125*, 4428−4429.
(30) Li, S. D.; Miao, C. Q.; Guo, J. C.; Ren, G. M. Carbon boronyls: Species with higher viable possibility than boron carbonyls at the density functional theory. *J. Comput. Chem.* **2005**, *26*, 799−802.
(31) Alexandrova, A. N.; Boldyrev, A. I.; Zhai, H. J.; Wang, L. S. All-boron aromatic clusters as potential new inorganic ligands and building blocks in chemistry. *Coord. Chem. Rev.* **2006**, *250*, 2811−2866.
(32) Yang, Y. G.; Jia, D. M.; Wang, Y. J.; Zhai, H. J.; Man, Y.; Li, S. D. A universal mechanism of the planar boron rotors B_{11}^-, B_{13}^+, B_{15}^+, and B_{19}^-: inner wheels rotating in pseudo-rotating outer bearings. *Nanoscale* **2017**, *9*, 1443−1448.
(33) Martinez-Guajardo, G.; Sergeeva, A. P.; Boldyrev, A. I.; Heine, T.; Ugalde, J. M.; Merino, G. Unravelling phenomenon of internal rotation in B_{13}^+ through chemical bonding analysis. *Chem. Commun.* **2011**, *47*, 6242−6244.
(34) Zhang, J.; Sergeeva, A. P.; Sparta, M.; Alexandrova, A. N. B_{13}^+: A photodriven molecular wankel engine. *Angew. Chem., Int. Ed.* **2012**, *51*, 8512−8515.
(35) Ruatta, S. A.; Hanley, L.; Anderson, S. L. Dynamics of boron cluster ion reactions with deuterium: Adduct formation and decay. *J. Chem. Phys.* **1989**, *91*, 226−239.
(36) Sowa-Resat, M. B.; Smolanoff, J.; Lapicki, A.; Anderson, S. L. Interaction of small boron cluster ions with HF. *J. Chem. Phys.* **1997**, *106*, 9511−9522.
(37) Hintz, P. A.; Sowa, M. B.; Ruatta, S. A.; Anderson, S. L. Reactions of boron cluster ions (B_n^+, n = 2−24) with N_2O: NO versus NN bond activation as a function of size. *J. Chem. Phys.* **1991**, *94*, 6446−6458.
(38) Ruatta, S. A.; Hintz, P. A.; Anderson, S. L. Boron cluster ion oxidation: Reactions with CO_2, dissociation of boron cluster oxide (B_nO^+) ions, and sequential oxidation. *J. Chem. Phys.* **1991**, *94*, 2833−2847.
(39) Hintz, P. A.; Ruatta, S. A.; Anderson, S. L. Interaction of boron cluster ions with water: Single collision dynamics and sequential etching. *J. Chem. Phys.* **1990**, *92*, 292−303.
(40) Hanley, L.; Anderson, S. L. Oxidation of small boron cluster ions (B_{1-13}^+) by oxygen. *J. Chem. Phys.* **1988**, *89*, 2848−2860.
(41) Wu, X. N.; Xu, B.; Meng, J. H.; He, S. G. C-H bond activation by nanosized scandium oxide clusters in gas-phase. *Int. J. Mass Spectrom.* **2012**, *310*, 57−64.
(42) Yuan, Z.; Zhao, Y. X.; Li, X. N.; He, S. G. Reactions of $V_4O_{10}^+$ cluster ions with simple inorganic and organic molecules. *Int. J. Mass Spectrom.* **2013**, *354−355*, 105−112.
(43) O'Hair, R. A. J. The 3D quadrupole ion trap mass spectrometer as a complete chemical laboratory for fundamental gas-phase studies of metal mediated chemistry. *Chem. Commun.* **2006**, 1469−1481.
(44) Socaciu, L. D.; Hagen, J.; Heiz, U.; Bernhardt, T. M.; Leisner, T.; Wöste, L. Reaction mechanism for the oxidation of free silver dimers. *Chem. Phys. Lett.* **2001**, *340*, 282−288.

https://doi.org/10.1021/jacs.4c07680
J. Am. Chem. Soc. 2024, 146, 31464−31471

(45) Chen, J. J.; Wang, S. D.; Li, Z. Y.; Li, X. N.; He, S. G. Selective reduction of NO into N_2 catalyzed by Rh_1-doped cluster anions $RhCe_2O_{3-5}^-$. *J. Am. Chem. Soc.* **2023**, *145*, 18658−18667.

(46) Kummerlöwe, G.; Beyer, M. K. Rate estimates for collisions of ionic clusters with neutral reactant molecules. *Int. J. Mass Spectrom.* **2005**, *244*, 84−90.

(47) Adamo, C.; Barone, V. Toward reliable density functional methods without adjustable parameters: The PBE0 model. *J. Chem. Phys.* **1999**, *110*, 6158−6170.

(48) Krishnan, R.; Binkley, J. S.; Seeger, R.; Pople, J. A. Self-consistent molecular orbital methods. XX. A basis set for correlated wave functions. *J. Chem. Phys.* **1980**, *72*, 650−654.

(49) Frisch, M. J.; Trucks, G. W.; Schlegel, H. B.; Scuseria, G. E.; Robb, M. A.; Cheeseman, J. R.; Scalmani, G.; Barone, V.; Petersson, G. A.; Nakatsuji, H.; Li, X.; Caricato, M.; Marenich, A. V.; Bloino, J.; Janesko, B. G.; Gomperts, R.; Mennucci, B.; Hratchian, H. P.; Ortiz, J. V.; Izmaylov, A. F.; Sonnenberg, J. L.; Williams-Young, D.; Ding, F.; Lipparini, F.; Egidi, F.; Goings, J.; Peng, B.; Petrone, A.; Henderson, T.; Ranasinghe, D.; Zakrzewski, V. G.; Gao, J.; Rega, N.; Zheng, G.; Liang, W.; Hada, M.; Ehara, M.; Toyota, K.; Fukuda, R.; Hasegawa, J.; Ishida, M.; Nakajima, T.; Honda, Y.; Kitao, O.; Nakai, H.; Vreven, T.; Throssell, K.; Montgomery, J. A.; Peralta, J. E.; Ogliaro, F.; Bearpark, M. J.; Heyd, J. J.; Brothers, E. N.; Kudin, K. N.; Staroverov, V. N.; Keith, T. A.; Kobayashi, R.; Normand, J.; Raghavachari, K.; Rendell, A. P.; Burant, J. C.; Iyengar, S. S.; Tomasi, J.; Cossi, M.; Millam, J. M.; Klene, M.; Adamo, C.; Cammi, R.; Ochterski, J. W.; Martin, R. L.; Morokuma, K.; Farkas, O.; Foresman, J. B.; Fox, D. J. *Gaussian 16*; Gaussian, Inc.: Wallingford CT, 2016.

(50) Chen, Q.; Li, W. L.; Zhao, Y. F.; Zhang, S. Y.; Hu, H. S.; Bai, H.; Li, H. R.; Tian, W. J.; Lu, H. G.; Zhai, H. J.; Li, S. D.; Li, J.; Wang, L. S. Experimental and theoretical evidence of an axially chiral borospherene. *ACS Nano* **2015**, *9*, 754−760.

(51) Zhai, H. J.; Zhao, Y. F.; Li, W. L.; Chen, Q.; Bai, H.; Hu, H. S.; Piazza, Z. A.; Tian, W. J.; Lu, H. G.; Wu, Y. B.; Mu, Y. W.; Wei, G. F.; Liu, Z. P.; Li, J.; Li, S. D.; Wang, L. S. Observation of an all-boron fullerene. *Nat. Chem.* **2014**, *6*, 727−731.

(52) Jian, T.; Chen, X. N.; Li, S. D.; Boldyrev, A. I.; Li, J.; Wang, L. S. Probing the structures and bonding of size-selected boron and doped-boron clusters. *Chem. Soc. Rev.* **2019**, *48*, 3550−3591.

(53) Fagiani, M. R.; Song, X.; Petkov, P.; Debnath, S.; Gewinner, S.; Schöllkopf, W.; Heine, T.; Fielicke, A.; Asmis, K. R. Structure and fluxionality of B_{13}^+ probed by infrared photodissociation spectroscopy. *Angew. Chem., Int. Ed.* **2017**, *56*, 501−504.

(54) Purvis, G. D.; Bartlett, R. J. A full coupled-cluster singles and doubles model: The inclusion of disconnected triples. *J. Chem. Phys.* **1982**, *76*, 1910−1918.

(55) Scuseria, G. E.; Schaefer, H. F. Is coupled cluster singles and doubles (CCSD) more computationally intensive than quadratic configuration interaction (QCISD)? *J. Chem. Phys.* **1989**, *90*, 3700−3703.

(56) Scuseria, G. E.; Janssen, C. L.; Schaefer, H. F. An efficient reformulation of the closed-shell coupled cluster single and double excitation (CCSD) equations. *J. Chem. Phys.* **1988**, *89*, 7382−7387.

(57) Lee, T. J.; Taylor, P. R. A diagnostic for determining the quality of single-reference electron correlation methods. *Int. J. Quantum Chem.* **2009**, *36*, 199−207.

(58) Gonzalez, C.; Schlegel, H. B. An improved algorithm for reaction path following. *J. Chem. Phys.* **1989**, *90*, 2154−2161.

(59) Gonzalez, C.; Schlegel, H. B. Reaction path following in mass-weighted internal coordinates. *J. Phys. Chem.* **1990**, *94*, 5523−5527.

(60) VandeVondele, J.; Krack, M.; Mohamed, F.; Parrinello, M.; Chassaing, T.; Hutter, J. Quickstep: Fast and accurate density functional calculations using a mixed Gaussian and plane waves approach. *Comput. Phys. Commun.* **2005**, *167*, 103−128.

(61) Goedecker, S.; Teter, M.; Hutter, J. Separable dual-space Gaussian pseudopotentials. *Phys. Rev. B: Condens. Matter Mater. Phys.* **1996**, *54*, 1703−1710.

(62) Li, W. L.; Chen, K. X.; Rossomme, E.; Head-Gordon, M.; Head-Gordon, T. Optimized pseudopotentials and basis sets for semiempirical density functional theory for electrocatalysis applications. *J. Phys. Chem. Lett.* **2021**, *12*, 10304−10309.

(63) Tkachenko, N. V.; Boldyrev, A. I. Chemical bonding analysis of excited states using the adaptive natural density partitioning method. *Phys. Chem. Chem. Phys.* **2019**, *21*, 9590−9596.

(64) Ziegler, T.; Rauk, A. On the calculation of bonding energies by the Hartree Fock Slater method: I. The transition state method. *Theor. Chim. Acta* **1977**, *46*, 1−10.

(65) Mitoraj, M. P.; Michalak, A.; Ziegler, T. A combined charge and energy decomposition scheme for bond analysis. *J. Chem. Theory Comput.* **2009**, *5*, 962−975.

(66) Mitoraj, M.; Michalak, A. Donor-acceptor properties of ligands from the natural orbitals for chemical valence. *Organometallics* **2007**, *26*, 6576−6580.

(67) Te Velde, G.; Bickelhaupt, F. M.; Baerends, E. J.; Fonseca Guerra, C.; Van Gisbergen, S. J. A.; Snijders, J. G.; Ziegler, T. Chemistry with ADF. *J. Comput. Chem.* **2001**, *22*, 931−967.

(68) Heully, J.-L.; Lindroth, I.; Lindroth, E.; Lundqvist, S.; Martensson-Pendrill, A. M. Diagonalisation of the Dirac Hamiltonian as a basis for a relativistic many-body procedure. *J. Phys. B: At. Mol. Phys.* **1986**, *19*, 2799−2815.

(69) Chang, C.; Pelissier, M.; Durand, P. Regular two-component Pauli-like effective-Hamiltonians in Dirac theory. *Phys. Scr.* **1986**, *34*, 394−404.

(70) VanLenthe, E.; VanLeeuwen, R.; Baerends, E. J.; Snijders, J. G. Relativistic regular two-component Hamiltonians. *J. Chem. Phys.* **1996**, *57*, 281−293.

(71) Cheng, X.; Li, Z. Y.; Mou, L. H.; Wei, G. P.; Liu, Q. Y.; He, S. G. Size-dependent reactivity of rhodium deuteride cluster anions $Rh_3D_n^-$ (n = 0−3) toward dinitrogen: The prominent role of σ donation. *J. Chem. Phys.* **2022**, *156*, 064303.

(72) Neumaier, M.; Weigend, F.; Hampe, O.; Kappes, M. M. Binding energies of CO on gold cluster cations Au_n^+ (n = 1−65): A radiative association kinetics study. *J. Chem. Phys.* **2005**, *122*, 104702.

(73) Neumaier, M.; Weigend, F.; Hampe, O.; Kappes, M. M. Binding energy and preferred adsorption sites of CO on gold and silver-gold cluster cations: Adsorption kinetics and quantum chemical calculations. *Faraday Discuss.* **2008**, *138*, 393−406.

(74) Steinfeld, J. I.; Francisco, J. S.; Hase, W. L. *Chemical Kinetics and Dynamics*; Prentice-Hall: Upper Saddle River, NJ, 1999; pp 231−313.

(75) Braunschweig, H.; Dewhurst, R. D.; Hupp, F.; Nutz, M.; Radacki, K.; Tate, C. W.; Vargas, A.; Ye, Q. Multiple complexation of CO and related ligands to a main-group element. *Nature* **2015**, *522*, 327−330.

(76) Zhai, H. J.; Kiran, B.; Li, J.; Wang, L. S. Hydrocarbon analogues of boron clusters−planarity, aromaticity and antiaromaticity. *Nat. Mater.* **2003**, *2*, 827−833.

https://doi.org/10.1021/jacs.4c07680
J. Am. Chem. Soc. 2024, 146, 31464−31471